Gyrokinetic particle simulations of the effects of compressional magnetic perturbations on drift-Alfvenic instabilities in tokamaks

Ge Dong,[1] Jian Bao,[2] Amitava Bhattacharjee,[1] Alain Brizard,[3] Zhihong Lin,[2,a)] and Peter Porazik[1]
[1]Department of Astrophysical Sciences and Princeton Plasma Physics Laboratory, Princeton, New Jersey 08543, USA
[2]Department of Physics and Astronomy, University of California, Irvine, California 92697, USA
[3]Department of Physics, Saint Michael's College, Colchester, Vermont 05439, USA

(Received 24 January 2017; accepted 15 May 2017; published online 10 August 2017)

The compressional component of magnetic perturbation $\delta B_\parallel$ can play an important role in drift-Alfvenic instabilities in tokamaks, especially as the plasma β increases (β is the ratio of kinetic pressure to magnetic pressure). In this work, we have formulated a gyrokinetic particle simulation model incorporating $\delta B_\parallel$, and verified the model in kinetic Alfven wave simulations using the Gyrokinetic Toroidal Code in slab geometry. Simulations of drift-Alfvenic instabilities in tokamak geometry shows that the kinetic ballooning mode (KBM) growth rate decreases more than 20% when $\delta B_\parallel$ is neglected for $\beta_e = 0.02$, and that $\delta B_\parallel$ has stabilizing effects on the ion temperature gradient instability, but negligible effects on the collisionless trapped electron mode. The KBM growth rate decreases about 15% when equilibrium current is neglected. *Published by AIP Publishing.* [http://dx.doi.org/10.1063/1.4997788]

I. INTRODUCTION

In theoretical and computational studies of toroidal plasmas using the kinetic approach, compressional magnetic perturbations $\delta B_\parallel$ have generally been neglected for plasma $\beta \ll 1$,[1] where β is the ratio between plasma kinetic pressure and magnetic pressure. However, even for small values of β, the $\delta B_\parallel$ effect can be important for plasma instabilities[2,3] such as the kinetic ballooning mode (KBM)[4] since it cancels out the stabilizing "drift-reversal" effects of the guiding center grad-B drifts associated with the perpendicular diamagnetic current in finite-β plasmas.[5] Local gyrokinetic simulations using GS2 (Ref. 2) and GYRO[6] show that the KBM growth rate can be reduced significantly when $\delta B_\parallel$ is neglected for electron β values as small as 2% ($\beta_e = 0.02$).

In this work, we have formulated and verified a gyrokinetic particle simulation model incorporating $\delta B_\parallel$. When the finite β effects are considered, the second order terms in the perturbed guiding center Hamiltonian contribute to extra polarization terms in the field equations.[7–9] At equilibrium and isotropic temperature, the conventional form of the component of Ampere's law parallel to the equilibrium magnetic field (hereafter, simply referred to as the parallel Ampere's law) is valid for arbitrary β. The perpendicular Ampere's law and gyrokinetic Poisson's equation become coupled for finite β. We have implemented this complete gyrokinetic simulation model incorporating $\delta B_\parallel$ in the Gyrokinetic Toroidal Code (GTC),[10] including the effects of the parallel equilibrium current density.[11] We have verified the implementation by showing that the effects of $\delta B_\parallel$ on the kinetic Alfven wave (KAW) from GTC simulations agree with the analytic dispersion relation in slab geometry. The GTC simulation of drift-Alfvenic instabilities in tokamak shows that the KBM growth rate decreases more than 20% when $\delta B_\parallel$ is neglected for $\beta_e = 0.02$, but that $\delta B_\parallel$ has negligible effects on the collisionless trapped electron mode (CTEM). Near the instability threshold of the ion temperature gradient (ITG) instability at $\beta_e = 0.01$, $\delta B_\parallel$ has stabilizing effects on the ITG mode. We also find that the KBM growth rate decreases about 15% when equilibrium current is neglected. We note that the equilibrium current in tokamak, which is mostly a parallel current and much larger than the perpendicular diamagnetic current, is neglected in most gyrokinetic simulations.

The outline of this paper is as follows; the formulation of the gyrokinetic Vlasov-Maxwell equations including $\delta B_\parallel$ terms is presented in Sec. II, followed by verification of KAW simulations in Sec. III. In Sec. IV, we present tokamak KBM simulation results illustrating the effects of $\delta B_\parallel$ and equilibrium current. In Sec. V, we summarize the main results and discuss future studies.

II. FORMULATION OF GYROKINETIC SIMULATIONS WITH $\delta B_\parallel$

A. Gyrokinetic Vlasov equations

The gyrokinetic equation for low frequency waves in magnetized plasmas[7] with a distribution function for the s species $F_s^{gyro} = f_s(\mathbf{R}, v_\parallel, \mu, t)$ in five-dimensional phase space is

$$\frac{d}{dt} f_s(\mathbf{R}, v_\parallel, \mu, t) = \left(\frac{\partial}{\partial t} + \dot{\mathbf{R}} \cdot \nabla + \dot{v}_\parallel \frac{\partial}{\partial v_\parallel} - \mathcal{C}_s\right) f_s = 0. \quad (1)$$

Here, the gyrocenter position $\mathbf{R}$, the magnetic moment μ and the parallel velocity $v_\parallel$ are the set of independent

a)Author to whom correspondence should be addressed: zhihongl@uci.edu

variables, and C_s denotes the collision operator, which is neglected in the following formulation for simplicity. The gyrocenter velocity $\dot{\mathbf{R}}$ and the parallel acceleration $\dot{v}_\parallel$ are

$$\dot{\mathbf{R}} = v_\parallel \frac{\mathbf{B}_0^* + \delta\mathbf{B}_\perp}{B_0^*} + \mathbf{v}_\mathbf{E} + \mathbf{v}_\mathbf{d} + \mathbf{v}_{\mathbf{b}\parallel}, \tag{2}$$

$$\dot{v}_\parallel = -\frac{1}{m_s}\frac{\mathbf{B}_0^* + \delta\mathbf{B}_\perp}{B_0} \cdot \left(\mu\nabla B_0 + Z_s\nabla\langle\phi\rangle - Z_s\nabla\frac{\langle\delta\mathbf{A}_\perp\cdot\mathbf{v}_\perp\rangle}{c}\right) - \frac{Z_s}{m_s c}\frac{\partial\langle\delta A_\parallel\rangle}{\partial t}. \tag{3}$$

In the above equations, $\mathbf{B}_0 = B_0\mathbf{b}_0$ is the equilibrium magnetic field, $\mathbf{B}_0^* = \mathbf{B}_0 + \frac{B_0 v_\parallel m_s c}{Z_s B_{0*}}\nabla\times\mathbf{b}_0$ is the modified magnetic field for the equation of motion to conserve the phase space volume, $B_0^* = B_0 + \frac{v_\parallel m_s c}{Z_s}\mathbf{b}_0\cdot\nabla\times\mathbf{b}_0$, $\mathbf{v}_\perp$ is the perpendicular component of particle velocity, $\delta A_\parallel$ and $\delta\mathbf{A}_\perp$ denote the parallel and perpendicular components of the vector potential, respectively, $\delta\mathbf{B}_\perp = \nabla\times(A_\parallel\mathbf{b}_0)$, and $\delta B_\parallel = \mathbf{b}_0\cdot\nabla\times\delta\mathbf{A}_\perp$. The $E\times B$ velocity, the magnetic drift velocity, and the gradient drift caused by the perturbed parallel magnetic field are

$$\begin{aligned}\mathbf{v}_\mathbf{E} &= \frac{c\mathbf{b}_0\times\nabla\langle\delta\phi\rangle}{B_0^*},\\ \mathbf{v}_\mathbf{d} &= \frac{m_s v_\parallel^2}{Z_s B_0^*}\mathbf{b}_0\times(\mathbf{b}_0\cdot\nabla\mathbf{b}_0) + \frac{\mu}{Z_s B_0^*}\mathbf{b}_0\times\nabla B_0,\\ \mathbf{v}_{\mathbf{b}\parallel} &= -\frac{\mathbf{b}_0\times\nabla\langle\delta\mathbf{A}_\perp\cdot\mathbf{v}_\perp\rangle}{B_0^*},\end{aligned} \tag{4}$$

where $\langle\ldots\rangle = \frac{1}{2\pi}\oint\ldots d\zeta$ represents gyrophase averaging, with ζ as the gyrophase. Applying Stokes theorem, we have[12]

$$\langle\delta\mathbf{A}_\perp\cdot\mathbf{v}_\perp\rangle = -\frac{c}{Z_s}\mu\langle\langle\delta B_\parallel\rangle\rangle. \tag{5}$$

Here $\langle\langle\delta B_\parallel\rangle\rangle = \frac{1}{\pi\rho^2}\int_0^\rho r dr\int_0^{2\pi}\delta B_\parallel d\zeta$ is the gyro-surface averaging of the perturbed parallel magnetic field, where ρ is the gyroradius and r denotes the radial direction in local cylindrical coordinates. In Fourier space, we have $\langle\langle\delta B_\parallel\rangle\rangle = \delta B_\parallel\frac{2}{k_\perp\rho}J_1(k_\perp\rho)$. In the above equations, $\langle\delta A_\parallel\rangle$ and $\langle\phi\rangle$ are gyroaveraged for the ions,[13] and taken at the gyrocenter position for the electrons.

Although GTC has been verified for full-f simulation, here, we implement $\delta B_\parallel$ in the perturbative (δf) simulation[14–16] for higher computational efficiency. In the δf simulations, the distribution function can be decomposed into an equilibrium and a perturbed parts as: $f_s = f_{s0} + \delta f_s$ for each species. The equilibrium part is just the solution to the neoclassical problem, satisfying the gyrokinetic equation

$$\hat{L_0} f_{s0} = 0, \tag{6}$$

where we define $\frac{d}{dt} = \hat{L} = \hat{L_0} + \delta\hat{L}$, and

$$\begin{aligned}\hat{L_0} &= \frac{\partial}{\partial t} + (v_\parallel\mathbf{b}_0 + \mathbf{v}_\mathbf{d})\cdot\nabla - \frac{\mu\mathbf{B}_0^*}{B_0}\cdot\nabla B_0\frac{\partial}{\partial v_\parallel},\\ \delta\hat{L} &= \left(\mathbf{v}_\mathbf{E} + \mathbf{v}_{\mathbf{b}\parallel} + \frac{v_\parallel\delta\mathbf{B}_\perp}{B_0^*}\right)\cdot\nabla - \left[\frac{\mu\delta\mathbf{B}_\perp\cdot\nabla B_0}{m_s B_0} + Z_s\frac{\mathbf{B}_0^* + \delta\mathbf{B}_\perp}{m_s B_0}\cdot\left(\nabla\phi - \nabla\frac{\langle\delta\mathbf{A}_\perp\cdot\mathbf{v}_\perp\rangle}{c}\right) + \frac{Z_s}{m_s c}\frac{\partial\langle\delta A_\parallel\rangle}{\partial t}\right]\frac{\partial}{\partial v_\parallel}.\end{aligned}$$

With the equilibrium solution from Eq. (6), we obtain

$$\begin{aligned}\hat{L}\frac{\delta f_s}{f_s} &= -\frac{f_{s0}}{f_s}\frac{\delta\hat{L}f_{s0}}{f_{s0}} = \left(1 - \frac{\delta f_s}{f_s}\right)\\ &\times\left[-\left(v_\parallel\frac{\delta\mathbf{B}_\perp}{B_0^*} + \mathbf{v}_\mathbf{E} + \mathbf{v}_{\mathbf{b}\parallel}\right)\cdot\frac{\nabla f_{s0}}{f_{s0}}\right.\\ &+\left(\frac{\mu\delta\mathbf{B}_\perp\cdot\nabla B_0}{B_0} + Z_s\frac{\mathbf{B}_0^* + \delta\mathbf{B}_\perp}{B_0}\right.\\ &\left.\left.\cdot\left(\nabla\phi - \nabla\frac{\langle\delta\mathbf{A}_\perp\cdot\mathbf{v}_\perp\rangle}{c}\right) + \frac{Z_s}{c}\frac{\partial\langle\delta A_\parallel\rangle}{\partial t}\right)\frac{1}{m_s f_{s0}}\frac{\partial f_{s0}}{\partial v_\parallel}\right].\end{aligned} \tag{7}$$

B. Gyrokinetic Maxwell equations

In order to derive the gyrokinetic Maxwell equations, it is convenient to use the transformation from the guiding center to the particle distribution. In isotropic plasmas, we have the expression for guiding center phase-space transformation as in Ref. 8, Eq. (41)

$$\begin{aligned}\delta f_s(\mathbf{x}, v_\parallel, \mu, t) = \int d\mathbf{R}\Big[&\delta F_s^{gyro}(\mathbf{R}, v_\parallel, \mu, t)\\ &+\frac{q_s}{T_s}\left(-\frac{\langle\delta\mathbf{A}_\perp\cdot\mathbf{v}_\perp\rangle}{c} + \langle\delta\phi\rangle - \delta\phi(\mathbf{R})\right)\\ &\times F_M(\mathbf{R}, v_\parallel, \mu, t)\Big]\boldsymbol{\delta}(\mathbf{x} - \mathbf{R} - \rho),\end{aligned} \tag{8}$$

where $\mathbf{x}$ denotes coordinates of the particle position, $\mathbf{R}$ denotes coordinates of the guiding center position, F_M is the local Maxwellian distribution, and

$$\langle\delta\phi\rangle = \frac{1}{2\pi}\int_0^{2\pi} d\zeta\int d\mathbf{x}'\delta\phi(\mathbf{x}')\delta(\mathbf{x}' - \mathbf{R} - \rho).$$

The quasi-neutrality condition in the particle coordinates is in the form of Eq. (44) in Ref. 8

$$\begin{aligned}&\frac{Z_i^2 n_i}{T_i}\left(\delta\phi - \tilde{\delta\phi}\right) - \frac{1}{B_0}\left(Z_i n_{i0}\{\delta B_\parallel\}_i - e n_{e0}\{\delta B_\parallel\}_e\right)\\ &\quad = Z_i n_i - e n_e,\end{aligned} \tag{9}$$

where $\tilde{\delta\phi}$ denotes double gyroaveraging

$$\tilde{\delta\phi} = \int d\mathbf{v}\int d\mathbf{R}\langle\delta\phi\rangle(\mathbf{R})F_M(\mathbf{R}, v_\parallel, \mu, t)\delta(\mathbf{x} - \mathbf{R} - \rho),$$

δn_s is the gyroaveraged particle density,

$$\delta n_s = \int d\mathbf{v}\int d\mathbf{R}\delta F_s^{gyro}(\mathbf{R}, v_\parallel, \mu, t)\delta(\mathbf{x} - \mathbf{R} - \rho),$$

and $\{\delta B_\parallel\}_s$ is defined as

$$\{\delta B_\parallel\}_s = \frac{m\Omega_s^2}{2\pi T_s}\int d\mathbf{v}\int d\mathbf{R}\int_0^\rho r'dr'\int_0^{2\pi} d\zeta'\int d\mathbf{x}'\delta B_\parallel(\mathbf{x}') \times \delta(\mathbf{x}'-\mathbf{R}-\rho)F_M\delta(\mathbf{x}-\mathbf{R}-\rho).$$

The velocity-space integral in the above equations is defined as

$$\int d\mathbf{v} = \frac{B_0}{m_s}\int_0^\infty d\mu\int_{-\infty}^\infty dv_\parallel\int_0^{2\pi} d\zeta.$$

For a single $k_\perp$ mode, the gyroaveraging and integrations over phase space can be represented using Bessel functions

$$\tilde{\delta\phi} = \delta\phi I_0(k_\perp^2\rho_s^2)\exp(-k_\perp^2\rho_s^2),$$
$$\{\delta B_\parallel\}_\alpha = \delta B_\parallel\left[I_0(k_\perp^2\rho_s^2) - I_1(k_\perp^2\rho_s^2)\right]\exp(-k_\perp^2\rho_s^2).$$

The parallel Ampere's law for $\delta A_\parallel$ is not modified by $\delta B_\parallel$, and is in the form of

$$\nabla_\perp^2 A_\parallel = \frac{4\pi}{c}\left(en_e\delta u_{\parallel e} - q_i n_i\delta u_{\parallel i}\right), \tag{10}$$

where the perturbed current is

$$n_\alpha\delta u_{\alpha\parallel} = \int d\mathbf{v}v_\parallel\int d\mathbf{R}\delta F_\alpha^{gyro}(\mathbf{R})\delta(\mathbf{x}-\mathbf{R}-\rho).$$

Equation (10) is valid only for isotropic plasmas. With anisotropic temperature, the parallel Ampere's law would include extra terms proportional to $T_\perp - T_\parallel$, which might be significant when $\beta_\parallel - \beta_\perp$ is of the order unity.[9]

Assuming that the perpendicular wave vector of the perturbed fields is much larger than the curvature of the equilibrium magnetic fields, the perpendicular Ampere's law for $\delta B_\parallel$ is

$$\nabla_\perp\delta B_\parallel\times\mathbf{b}_0 = \frac{4\pi}{c}\left(Z_i\int d\mathbf{v}\mathbf{v}_\perp\delta f_i - e\int d\mathbf{v}\mathbf{v}_\perp\delta f_e\right). \tag{11}$$

Using Stokes' theorem

$$-\oint f\frac{\mathbf{v}_\perp}{\Omega}d\zeta = \oint fd\mathbf{l} = \int_s d\mathbf{S}\times\nabla f = -\int rdr\int d\zeta\mathbf{b}\times\nabla f,$$

and assuming $1/k_\perp L \ll 1$, the $\mathbf{b}\times\nabla$ operator can be taken out of the integral and removed from the perpendicular Ampere's law. After transformation from guiding center coordinates to particle coordinates [Eq. (8)], we get

$$\begin{aligned}&\frac{\delta B_\parallel B_0}{4\pi} + 2\pi\Omega_e^2\int d\mu dv_\parallel\left[B_0\left\langle\int_0^{\rho_e}F_e^{gyro}rdr\right\rangle\right.\\ &\left.+\frac{f_M}{\rho_e^2}\left\langle\int_0^{\rho_e}\left\langle\int_0^{\rho_e}\delta B_\parallel r'dr'\right\rangle rdr\right\rangle\right]\\ &= -2\pi\Omega_i^2\int d\mu dv_\parallel\left[B_0\left\langle\int_0^{\rho_i}\left(F_i^{gyro}+\frac{e\langle\delta\phi\rangle - e\delta\phi}{T_i}F_M\right)rdr\right\rangle\right.\\ &\left.+\frac{F_M}{\rho_i^2}\left\langle\int_0^{\rho_i}\left\langle\int_0^{\rho_i}\delta B_\parallel r'dr'\right\rangle rdr\right\rangle\right].\end{aligned} \tag{12}$$

For a single $k_\perp$ mode and $k_\perp\rho_e \ll 1$ we obtain

$$\begin{aligned}&\frac{\delta B_\parallel B_0\{1+\beta_e+\beta_i\left[I_0\left(k_\perp^2\rho_i^2\right) - I_1\left(k_\perp^2\rho_i^2\right)\right]\exp\left(-k_\perp^2\rho_i^2\right)\}}{8\pi}\\ &+\frac{\beta_i B_0^2 e\delta\phi}{16\pi T_i}\left\{\left[I_0\left(k_\perp^2\rho_i^2\right) - I_1\left(k_\perp^2\rho_i^2\right)\right]\exp\left(-k_\perp^2\rho_i^2\right) - 1\right\}\\ &= -\pi\Omega_e^2\int d\mu dv_\parallel B_0\int_0^{\rho_e}F_e^{gyro}rdr - \pi\Omega_i^2\\ &\times\int d\mu dv_\parallel B_0\left\langle\int_0^{\rho_i}F_i^{gyro}rdr\right\rangle.\end{aligned} \tag{13}$$

When $k_\perp\rho_i \ll 1$, Eq. (13) reduces to

$$\frac{\delta B_\parallel B_0(1+\beta_e+\beta_i)}{4\pi} = -\delta P_{e\perp} - \delta P_{i\perp}, \tag{14}$$

where $\delta P_{s\perp} = \frac{2\pi B_0}{m_s}\int d\mu dv_\parallel\delta f_s\mu B_0$, $\beta_s = 8\pi n_{s0}T_{s0}/B_0^2$ for each species. Equations (2) and (3), (7), (9), (10), and (12) form the closed system of equations for the nonlinear gyrokinetic simulations.

C. Fluid kinetic hybrid electron model with $\delta B_\parallel$

The formulation of $\delta B_\parallel$ for the gyrokinetic simulation is first implemented and verified in the framework of the fluid-kinetic hybrid electron model. The fluid-kinetic hybrid electron model is useful in circumventing the numerical challenges associated with the electron Courant condition and tearing modes.[16–19] For the purpose of verifying the implementation of $\delta B_\parallel$ in the gyrokinetic simulation, here, we use the fluid-kinetic hybrid electron model with $\delta B_\parallel$ for simulations of non-tearing modes including kinetic shear Alfven wave (KAW) and kinetic ballooning mode (KBM) as shown in Secs. III and IV, respectively. However, the implementation of $\delta B_\parallel$ in the fluid-kinetic hybrid electron model can be readily utilized for the GTC simulation of kink instability,[20] resistive[21] and collisionless tearing modes.[22]

Integrating the kinetic equation (1), we can get the electron continuity equation in the conservative form as

$$\frac{\partial\delta n_e}{\partial t} + \nabla\cdot\mathbf{\Gamma} = 0, \tag{15}$$

where $\mathbf{\Gamma} = \frac{2\pi}{m_e}\int dv_\parallel\int d\mu B_0^* F_e^{gyro}\dot{\mathbf{R}}$ is the particle flux and $\delta n_e = \frac{2\pi}{m_e}\int dv_\parallel\int d\mu B_0^*\delta F_e^{gyro}$ is the perturbed electron density. With the guiding center drift velocity $\dot{\mathbf{R}}$, the particle flux is

$$\begin{aligned}\mathbf{\Gamma} = n_0\left(u_{\parallel 0}+\delta u_\parallel\right)\frac{\mathbf{B}_0+\delta\mathbf{B}_\perp}{B_0} + \mathbf{v}_\mathbf{E}(n_0+\delta n_e)\\ -\frac{cP_\parallel\mathbf{b}_0\times(\mathbf{b}_0\cdot\nabla\mathbf{b}_0)}{eB_0} - \frac{cP_\perp\mathbf{b}_0\times\nabla B_0}{eB_0^2}\\ -\frac{cP_\perp\mathbf{b}_0\times\nabla\delta B_\parallel}{eB_0^2},\end{aligned} \tag{16}$$

where $u_{\parallel 0}$ is the equilibrium flow, $P_\perp = \int d\mathbf{v}\mu B_0 F_e^{gyro}$ and $P_\parallel = \int d\mathbf{v}mv_\parallel^2 F_e^{gyro}$ are perpendicular and parallel pressures respectively. With the equilibrium solution Eq. (6) and some algebra, the continuity equation becomes

$$\frac{\partial \delta n_e}{\partial t} + \mathbf{B}_0 \cdot \nabla\left(\frac{n_0 \delta u_{\parallel e}}{B_0}\right) + B_0 \mathbf{v}_E \cdot \nabla\left(\frac{n_0}{B_0}\right) - n_0(\mathbf{v}_* + \mathbf{v}_\mathbf{E}) \cdot \frac{\nabla B_0}{B_0} + \delta \mathbf{B}_\perp \cdot \nabla\left(\frac{n_0 u_{\parallel 0}}{B_0}\right)$$
$$- \frac{c\nabla \times \mathbf{B}_0}{eB_0^2} \cdot \left(\nabla \delta P_\parallel + \frac{(\delta P_\perp - \delta P_\parallel)\nabla B_0}{B_0} - n_0 e \nabla \delta\phi\right) + \nabla \cdot \left(\frac{c\delta P_\parallel \mathbf{b}_0 \nabla \times \mathbf{b}_0 \cdot \mathbf{b}_0}{eB_0}\right)$$
$$+ \delta \mathbf{B}_\perp \cdot \nabla\left(\frac{n_{0e} \delta u_{\parallel e}}{B_0}\right) + B_0 \mathbf{v}_\mathbf{E} \cdot \nabla\left(\frac{\delta n_e}{B_0}\right) + \frac{c\delta n_e}{B_0^2} \mathbf{b}_0 \times \nabla B_0 \cdot \nabla \delta\phi + \frac{c\delta n_e}{B_0^2} \nabla \times \mathbf{B}_0 \cdot \nabla \delta\phi$$
$$- \frac{c\mathbf{b}_0 \times \nabla \delta B_\parallel}{e} \cdot \nabla\left(\frac{\delta P_\perp + P_{\perp 0}}{B_0^2}\right) - \frac{c\nabla \times \mathbf{b}_0 \cdot \nabla \delta B_\parallel}{eB_0^2}(\delta P_\perp + P_{\perp 0}) = 0, \tag{17}$$

where the diamagnetic drift velocity is $\mathbf{v}_* = \frac{1}{n_0 m_e \Omega_e} \mathbf{b}_0 \times \nabla(\delta P_\parallel + \delta P_\perp)$.

The parallel electron fluid velocity $\delta u_{e\parallel}$ can be calculated by inverting the parallel Ampere's law, Eq. (10), where $\delta u_{i\parallel}$ is from the ion gyrokinetic equation and $\delta A_\parallel$ is from the time integration of

$$\frac{\partial \delta A_\parallel}{\partial t} = -c\delta E_\parallel - c\mathbf{b}_0 \cdot \nabla \delta\phi, \tag{18}$$

where $\delta\phi$ can be solved from Poisson's equation, and the parallel electric field $\delta E_\parallel$ can be solved by the iterative method as follows.

The effective potential is defined as: $-\mathbf{b}_0 \cdot \nabla \phi_{eff} = \delta E_\parallel$. The perturbed electron distribution function is separated into adiabatic and non-adiabatic responses

$$\frac{d}{dt} f_e = \hat{L} f_e = \left(\hat{L_0} + \delta\hat{L}\right)\left(F_M + \delta f_e^{(0)} + \delta h_e\right) = 0, \tag{19}$$

where

$$\mathbf{L}_0 = \frac{\partial}{\partial t} + \left(v_\parallel \mathbf{b}_0 + \mathbf{v}_\mathbf{d}\right) \cdot \nabla - \frac{\mu \mathbf{B}_0^*}{B_0} \cdot \nabla B_0 \frac{\partial}{\partial v_\parallel},$$
$$\delta L = \left(v_\parallel \frac{\delta \mathbf{B}_\perp}{B_0} + \mathbf{v}_\mathbf{E} + \mathbf{v}_{\mathbf{b}\parallel}\right) \cdot \nabla - \left(\frac{\mu}{m_e}\frac{\delta \mathbf{B}_\perp}{B_0} \cdot \nabla B_0 + \frac{e}{m_e} E_\parallel - \frac{\mu}{m_e} \mathbf{b}_0 \cdot \nabla \delta B_\parallel - \frac{e}{m_e}\frac{\mathbf{v}_\mathbf{c}}{v_\parallel} \cdot \nabla \phi + \frac{\mu}{m_e}\frac{\mathbf{v}_\mathbf{c}}{v_\parallel} \cdot \nabla \delta B_\parallel\right) \frac{\partial}{\partial v_\parallel}. \tag{20}$$

We define the electron adiabatic response $\delta f_e^{(0)}$ by the dominant $v_\parallel$ terms in the electron kinetic equation

$$\frac{v_\parallel \mathbf{B}_0 \cdot \nabla \delta f_e^{(0)}}{B_0} = -v_\parallel \frac{\delta \mathbf{B}_\perp}{B_0} \cdot \nabla F_M - \frac{\mu v_\parallel}{B_0 T_e} \delta \mathbf{B}_\perp \cdot \nabla B_0 F_M + \frac{e v_\parallel}{T_e} \mathbf{b}_0 \cdot \nabla \phi_{eff} F_M - \frac{\mu v_\parallel}{T_e} \mathbf{b}_0 \cdot \nabla \delta B_\parallel F_M. \tag{21}$$

Since we have

$$\delta \mathbf{B}_\perp = \nabla\psi \times \nabla\alpha - \nabla\psi_0 \times \nabla\alpha_0,$$

and

$$\nabla|_{v_\perp} F_M = \nabla|_\mu F_M + \frac{\mu \nabla B_0}{T_e} F_M,$$

we can solve for the adiabatic electron response $\delta f_e^{(0)}$ as

$$\delta f_e^{(0)} = \frac{e\phi_{eff}}{T_e} F_M - \frac{\mu}{T_e} \delta B_\parallel F_M + \frac{\partial F_M}{\partial \psi_0}\bigg|_{v_\perp} \delta\psi + \frac{\partial F_M}{\partial \alpha_0}\bigg|_{v_\perp} \delta\alpha. \tag{22}$$

Then, the lowest order effective potential $\delta\phi_{eff}^{(0)}$ can be found by integrating the above equation in velocity space

$$\frac{e\phi_{eff}^{(0)}}{T_e} = \frac{\delta n_e}{n_0} + \frac{\delta B_\parallel}{B_0} - \frac{\partial \ln n_0}{\partial \psi_0} \delta\psi - \frac{\partial \ln n_0}{\partial \alpha_0} \delta\alpha. \tag{23}$$

Using Eqs. (7), (9), (10), (12), (17), (18), and (23) along with the electron and ion orbit equations, we have a closed system for simulations with adiabatic electrons.

To incorporate electron kinetic effects, from Eqs. (19)–(21), we can get the δh_e equation for the non-adiabatic electron response as

$$\mathbf{L}\frac{\delta h_e}{f_e} = \frac{1}{f_e}\left(-\mathbf{L}_0 \delta f_e^{(0)} - \delta \mathbf{L} F_M\right) = \left(1 - \frac{\delta f_e^{(0)}}{F_M} - w\right)\left[-\frac{\partial}{\partial t}\frac{\delta f_e^{(0)}}{F_M} - \mathbf{v}_\mathbf{d} \cdot \nabla \frac{\delta f_e^{(0)}}{F_M} - \mathbf{v}_\mathbf{E} \cdot \nabla \ln F_M - \frac{m_e v_\parallel}{T_e}\frac{e}{m_e}\frac{\mathbf{v}_\mathbf{g}}{v_\parallel} \cdot \nabla \delta\phi F_M - \mathbf{v}_{\mathbf{b}_\parallel} \cdot \nabla \ln F_M + \frac{m_e v_\parallel}{T_e}\frac{\mu}{m_e}\frac{\mathbf{v}_\mathbf{g}}{v_\parallel} \cdot \nabla \delta B_\parallel F_M + \frac{m_e v_\parallel}{T_e}\frac{e}{m_e}\frac{\mathbf{v}_\mathbf{d}}{v_\parallel} \cdot \nabla \phi F_M - \frac{m_e v_\parallel}{T_e}\frac{\mu}{m_e}\frac{\mathbf{v}_\mathbf{d}}{v_\parallel} \cdot \nabla \delta B_\parallel F_M\right]$$
$$= \left(1 - \frac{\delta f_e^{(0)}}{F_M} - w\right)\left[-\frac{\partial}{\partial t}\frac{\delta f_e^{(0)}}{F_M} - \mathbf{v}_\mathbf{E} \cdot \nabla \ln F_M|_{v_\perp} + \frac{c\mu}{eB_0} \mathbf{b}_0 \times \nabla \delta B_\parallel \cdot \nabla \ln F_M|_{v_\perp} - \mathbf{v}_\mathbf{d} \cdot \nabla \frac{\delta f_e^{(0)}}{F_M} + \frac{e}{T_e} \mathbf{v}_\mathbf{d} \cdot \nabla \delta\phi - \frac{\mu}{T_e} \mathbf{v}_\mathbf{d} \cdot \nabla \delta B_\parallel\right]$$
$$= \left(1 - \frac{\delta f_e^{(0)}}{F_M} - w\right)\left[-\frac{\partial}{\partial t}\frac{\delta f_e^{(0)}}{F_M} - \mathbf{v}_\mathbf{E} \cdot \nabla \ln F_M|_{v_\perp} + \frac{c\mu}{eB_0} \mathbf{b}_0 \times \nabla \delta B_\parallel \cdot \nabla \ln F_M|_{v_\perp} - \mathbf{v}_\mathbf{d} \cdot \nabla\left(\frac{e\delta\phi_{ind}^{(0)}}{T_e} + \frac{\delta\psi}{f_{e0}}\frac{\partial f_{e0}}{\partial \psi_0}|_{v_\perp}\right)\right], \tag{24}$$

where the lowest order inductive potential is: $\delta\phi_{ind}^{(0)} = \phi_{eff}^{(0)} - \delta\phi$. We have ignored the nonlinear terms involving $\delta\mathbf{L}\delta f_e^{(0)}$.

Now, we have the first order correction in $\delta n_e^{(1)} = \int d\mathbf{v}\delta h_e$, which can be used for the first order correction for ϕ_{eff} [since $\delta B_\parallel$ is determined by Eq. (12)]

$$\frac{e\phi_{eff}^{(1)}}{T_e} = -\frac{\delta n_e^{(1)}}{n_0}. \tag{25}$$

Equations (24) and (25) can be iterated to get higher-order corrections to the electron non-adiabatic distribution function.

This formulation keeps the equilibrium current[11] terms, i.e., $u_{\parallel 0}$ and terms proportional to $\nabla \times \mathbf{B}_0$. The equilibrium current will have coupled terms with $\delta B_\parallel$ in the last term in electron continuity equation (17), as well as the ion weight equation through the curvature drive

$$\begin{aligned}\frac{d}{dt}\frac{\delta f_i}{f_i} = \left(1 - \frac{\delta f_i}{f_i}\right)\Bigg[&-\frac{c\mathbf{b}_0}{B_0}\times\nabla\left(\delta\phi - v_\parallel\lambda B_0 + \frac{\mu}{Z_i}\langle\langle\delta B_\parallel\rangle\rangle\right)\\ &\cdot\nabla\ln f_M|_{v_\perp} + \frac{Z_i}{T}v_\parallel E_\parallel - \frac{\mu v_\parallel \mathbf{b}_0\cdot\nabla\langle\langle\delta B_\parallel\rangle\rangle}{T}\\ &-\frac{Z_i}{T}\mathbf{v}_\mathbf{d}\cdot\nabla\left(\phi + \frac{\mu}{Z_i}\langle\langle\delta B_\parallel\rangle\rangle\right)\Bigg],\end{aligned} \tag{26}$$

where $\mathbf{v}_\mathbf{d} = \mathbf{v}_\mathbf{g} + \mathbf{v}_\mathbf{c} = \frac{c\mu}{Z_i B_0^2}\mathbf{B}_0\times\nabla B_0 + \frac{m_i c v_\parallel^2}{Z_i B_0^3}\mathbf{B}_0\times\nabla B_0 + \frac{m_i c v_\parallel^2}{Z_i B_0^2}\nabla\times\mathbf{B}_0$.

D. Simulation flow chart

The GTC flow chart of advancing the fluid-kinetic hybrid electron model from the nth to the $(n+1)$th time step is illustrated in Fig. 1. It includes 8 equations, corresponding to Eqs. (7), (9), (10), (12), (17), (18), (24), and (25). Similar procedures based on this flow chart without $\delta B_\parallel$ have already been extensively applied for GTC simulations of microturbulence,[23,24] energetic particle transport[25] and Alfven eigenmodes.[26,27]

In the first blue box are the main particle and field quantities at the nth time step. In the second pink box, we first time-advance the ion kinetic equation for δf_i. Each particle has a weight defined as $w_i = \delta f_i/f_i$ to represent its contribution to the perturbed distribution function. The evolution equation for this weight can be solved using the δf_i equation, Eq. (26). The gyro-averaging and gyro-surface averaging for the field quantities are performed using the gyrocenter position $\mathbf{R}$ and the perpendicular energy $\mu B_0(\mathbf{R})$. Numerically, the gyro-surface averaging is approximated as gyro-averaging over an effective orbit with radius $\rho/\sqrt{2}$.[12] The electron continuity equation for δn_e and the equation for $\delta A_\parallel$ are also advanced in this step. Using the parallel Ampere's law, along with the ion distribution and $\delta A_\parallel$, $\delta u_{e\parallel}$ at the $(n+1)$th time step can now be calculated. To incorporate the effects of non-adiabatic electron responses, the electron kinetic equation (24) is iterated with the time derivative of the lower order response, as shown in the third magenta box. This step also includes the correction of the effective potential $\delta\phi_{eff}$ by the non-adiabatic response, Eq. (25). Since we now have the complete electron and ion information at the $(n+1)$th time step, field equations can be solved as in the fourth orange box. The perpendicular Ampere's law and Poisson's equation are coupled. After solving for $\delta\phi$ and $\delta B_\parallel$, we have a set of new particle and field quantities to proceed to the $(n+2)$th time step.

III. VERIFICATION OF $\delta B_\parallel$ EFFECTS ON KINETIC ALFVEN WAVE

A. Analytic KAW dispersion relation

We first verify the implementation of $\delta B_\parallel$ by comparing GTC linear simulations of kinetic Alfven wave (KAW) with the analytic dispersion relation in the slab geometry. In the spectrum space, the set of linearized gyrokinetic equations in a uniform background with $Z_i = e$, $T_i = T_e$ become

$$\begin{aligned}\delta f_i &= \frac{k_\parallel v_\parallel}{\omega - k_\parallel v_\parallel}\frac{eF_M}{T}\left[J_0(k_\perp\rho_i)\delta\phi + \frac{2J_1(k_\perp\rho_i)}{k_\perp\rho_i}\frac{\mu\delta B_\parallel}{e} - J_0(k_\perp\rho_i)\frac{\omega}{ck_\parallel}\delta A_\parallel\right],\\ \delta f_e &= \frac{-k_\parallel v_\parallel}{\omega - k_\parallel v_\parallel}\frac{eF_M}{T}\left[\delta\phi - \frac{\mu\delta B_\parallel}{e} - \frac{\omega}{ck_\parallel}\delta A_\parallel\right],\\ &\frac{e^2 n_0}{T}\left[1 - I_0\left(k_\perp^2\rho_i^2\right)\exp\left(-k_\perp^2\rho_i^2\right)\right]\delta\phi - \frac{en_0}{B_0}\left[\left(I_0\left(k_\perp^2\rho_i^2\right) - I_1\left(k_\perp^2\rho_i^2\right)\right)\exp\left(-k_\perp^2\rho_i^2\right) - 1\right]\delta B_\parallel\\ &\quad = \frac{2\pi eB_0}{m_i}\int d\mu dv_\parallel\delta f_i J_0(k_\perp\rho_i) - \frac{2\pi eB_0}{m_e}\int d\mu dv_\parallel\delta f_e,\\ -k_\perp^2\delta A_\parallel &= \frac{8\pi^2 B_0 n_0 e}{c}\left[\frac{1}{m_e}\int d\mu dv_\parallel v_\parallel\delta f_e - \frac{1}{m_i}\int d\mu dv_\parallel v_\parallel\delta f_i\right],\\ &\frac{\delta B_\parallel\left\{1 + \beta_e + \beta_i\left[I_0\left(k_\perp^2\rho_i^2\right) - I_1\left(k_\perp^2\rho_i^2\right)\right]\exp\left(-k_\perp^2\rho_i^2\right)\right\}}{B_0} + \frac{\beta_i}{2}\frac{e\delta\phi}{T}\left\{\left[I_0\left(k_\perp^2\rho_i^2\right) - I_1\left(k_\perp^2\rho_i^2\right)\right]\exp\left(-k_\perp^2\rho_i^2\right) - 1\right\}\\ &\quad = -\beta_e\frac{\pi B_0^2}{n_0 T_0 m_e^2}\int d\mu dv_\parallel\mu\delta f_e - \beta_i\frac{\pi B_0^2}{n_0 T_0 m_i^2}\int d\mu dv_\parallel\mu\delta f_i\frac{2J_1(k_\perp\rho_i)}{k_\perp\rho_i}.\end{aligned}$$

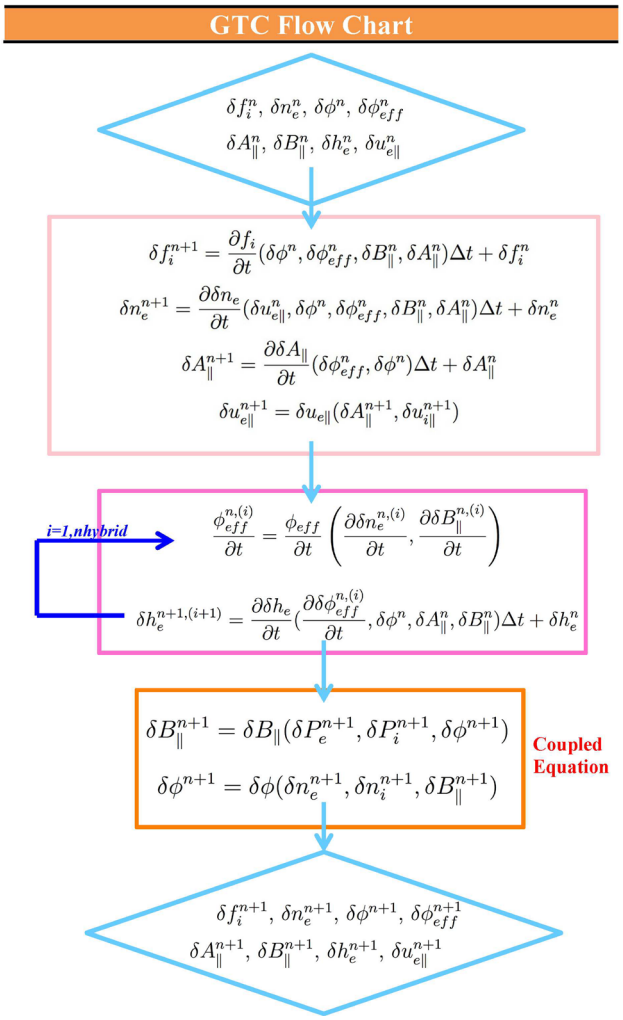

FIG. 1. GTC flow chart.

Combining the above equations, we get the dispersion relation

$$\left(\frac{k_\perp^2\rho_s^2 k_\parallel^2 v_A^2}{\omega^2}A - AB + B^2\right)\left(\frac{2A}{\beta_i} - AD + C^2\right) = (AE + BC)^2, \tag{27}$$

where

$$A = 1 + I_0(k_\perp^2\rho_s^2)\exp(-k_\perp^2\rho_s^2)\zeta_i Z(\zeta_i) + 1 + \zeta_e Z(\zeta_e),$$
$$B = 1 - I_0(k_\perp^2\rho_s^2)\exp(-k_\perp^2\rho_s^2),$$
$$C = \left[I_0(k_\perp^2\rho_s^2) - I_1(k_\perp^2\rho_s^2)\right]\exp(-k_\perp^2\rho_s^2)\zeta_i Z(\zeta_i) - \zeta_e Z(\zeta_e),$$
$$D = 2\left[I_0(k_\perp^2\rho_s^2) - I_1(k_\perp^2\rho_s^2)\right]\exp(-k_\perp^2\rho_s^2)\zeta_i Z(\zeta_i) + 2\zeta_e Z(\zeta_e),$$
$$E = \left[I_0(k_\perp^2\rho_s^2) - I_1(k_\perp^2\rho_s^2)\right]\exp(-k_\perp^2\rho_s^2) - 1.$$

This result agrees with the KAW dispersion relation derived in Ref. 28, in the limit of $k_\perp\rho_e \ll 1$. The dispersion relation Eq. (27) is plotted as the green solid line in Fig. 2, where $k_\perp\rho_s = 0.69$, β_e is scanned from 0.06 to 1.76.

B. Simulation results

In the simulations, the coupled equations for $\delta\phi$ and $\delta B_\parallel$ as shown in the orange box in the flow chart can be solved by a linear solver package such as PETSc.[29] For simplicity, in the KAW simulations, we first neglect the contribution of $\delta B_\parallel$ in Poisson's equation and the contribution of $\delta\phi$ in the perpendicular Ampere's law. The two equations become decoupled and can be solved by the PETSc package using electron and ion information at the $(n+1)$th time step. In that case, the dispersion relation becomes

$$\left(\frac{\omega^2}{k_\parallel^2 v_A^2} - \frac{k_\perp^2\rho_s^2}{B}\right)\left[(1 + Z(\zeta_e)\zeta_e) + (1 + Z(\zeta_i)\zeta_i) \times \exp(-k_\perp^2\rho_s^2)(1 - B) + \frac{\beta_e}{2}\delta_\parallel\right] = k_\perp^2\rho_s^2, \tag{28}$$

where

$$\delta_\parallel = \frac{\left[1 + Z(\delta_e)\zeta_e - (1 + Z(\zeta_i)\zeta_i)(E+1)\right]^2}{1 + \beta_e + \beta_i(E+1) - \left[1 + Z(\zeta_e)\zeta_e + (1 + Z(\zeta_i)\zeta_i)(E+1)\right]}.$$

When the compressional magnetic perturbation is neglected (i.e., setting $\delta B_\parallel = 0$), the $\delta_\parallel$ term is gone, and the dispersion relation becomes

$$\left(\frac{\omega^2}{k_\parallel^2 v_A^2} - \frac{k_\perp^2\rho_s^2}{B}\right)\left[(1 + Z(\zeta_e)\zeta_e) + (1 + Z(\zeta_i)\zeta_i) \times \exp(-k_\perp^2\rho_s^2)(1 - B)\right] = k_\perp^2\rho_s^2. \tag{29}$$

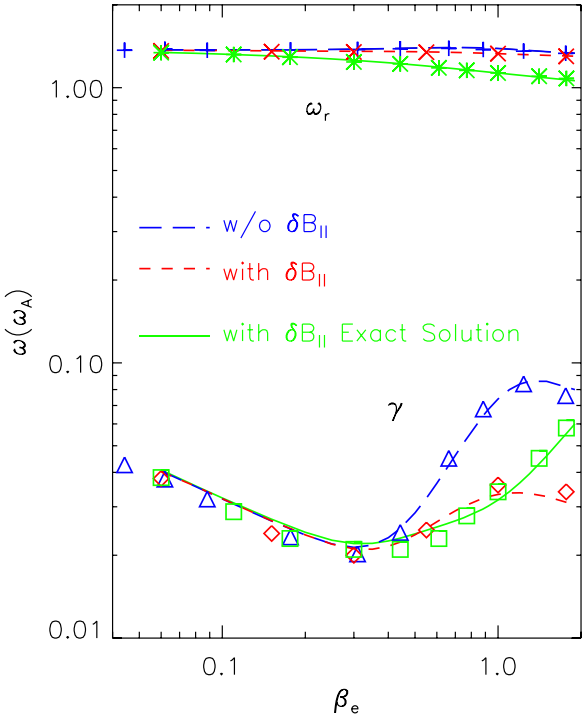

FIG. 2. KAW damping rate $-\gamma$ (triangle for simulations without $\delta B_\parallel$, diamond for simulations with $\delta B_\parallel$, without coupling terms, and square for simulations with $\delta B_\parallel$ and with coupling terms) and real frequency ω (plus sign for simulations without $\delta B_\parallel$, cross for simulations with $\delta B_\parallel$, without coupling terms, and star for simulations with $\delta B_\parallel$ and with coupling terms) vs β_e. The solid green lines represent the solution from the dispersion relation, Eq. (27). Dashed red lines represent the solution from Eq. (28), and long dashed blue lines represent the solution from Eq. (29).

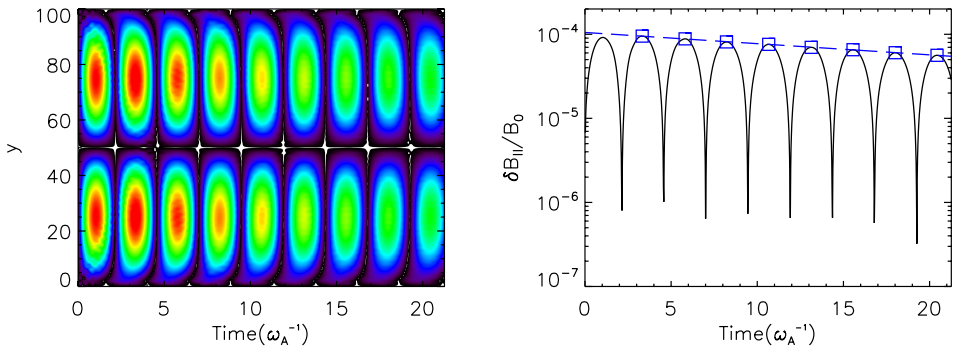

FIG. 3. Time history of $\delta B_\parallel(y,t)$, left panel. The y axis is in the unit of $0.091\rho_s$. The right panel is a cut at the wave peak ($\delta B_\parallel(r=75,t)$). The blue dashed line is a linear fit for the wave peaks.

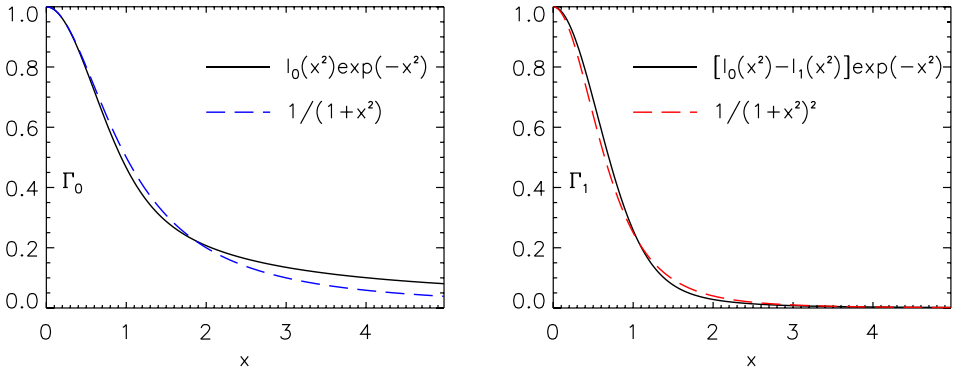

FIG. 4. Pade approximation (left) for Γ_0 and the approximation for Γ_1 (right). Solid lines are the exact expressions and dashed lines are the approximations.

The approximated dispersion relation Eqs. (28) and (29) are plotted as the dashed red line and the long dashed blue line, respectively, in Fig. 2. $\delta B_\parallel$ has a significant effect on the KAW damping rate for $\beta_e > 0.3$, and the coupling terms in Poisson's equation and perpendicular Ampere's law become important for the KAW damping rate, for $\beta_e > 1$.

In the GTC simulations, we use the fluid-kinetic hybrid electron model as introduced in Sec. II for a slab geometry, and $k_\perp\rho_s = 0.69$. Alfven frequency is defined as $\omega_A = k_\parallel v_A$. The β_e is scanned from 0.06 to 1.76. The time history of $|\delta B_\parallel|$ in the case of $\beta_e = 1.76$ is shown in Fig. 3. In this case, $\beta_e = 1.76$, $k_\perp\rho_s = 0.69$, $\omega_r = 1.30\omega_A$, $\gamma = -0.034k_\parallel v_A$.

Simulation results with $\delta B_\parallel$ using this model are plotted as red data points, and agree with the analytical results of Eq. (28), with an error within 1% for the real frequency and 5% for the damping rate. Simulation results without $\delta B_\parallel$ are plotted as blue data points and agree well with the analytical results of Eq. (29). In single $k_\perp$ simulations, the gyro-averaging and gyro-surface averaging in the field equations can be calculated analytically, and thus the perpendicular Ampere's law and Poisson's equation with coupling terms can be solved easily as algebraic equations. The simulation results of $\delta B_\parallel$ with the coupling terms using this method are plotted as green data points in Fig. 2, and agree well with the analytical results of Eq. (27).

IV. EFFECTS OF $\delta B_\parallel$ on DRIFT-ALFVENIC INSTABILITIES IN TOKAMAK

We now apply the complete gyrokinetic formulation to study the effects of $\delta B_\parallel$ on drift-Alfvenic instabilities in tokamak. Since the spectral method is not applicable in the toroidal geometry, we need to solve the Poisson equation and Ampere's law in the real space. The Pade approximation is used to solve Poisson's equation first. Then, the perpendicular Ampere's law is solved using $\delta\phi$ and an approximation for $\Gamma_1 = [I_0(x^2) - I_1(x^2)]\exp(-x^2) \simeq \frac{1}{(1+x^2)^2}$. The properties of the Pade approximation and the Γ_1 approximation are shown in Fig. 4. The maximum error in the Γ_1 approximation: $max(|\Gamma_1 - \frac{1}{(1+x^2)^2}|)$ is 5%. After these approximations, the coupled equations are in the form of

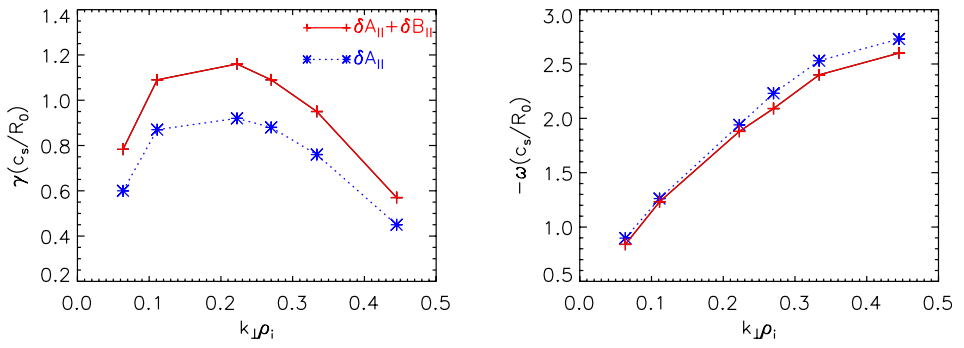

FIG. 5. KBM growth rate γ (left) and real frequency ω (right) vs poloidal mode number $k_\perp$ for $\beta_e = 0.02$.

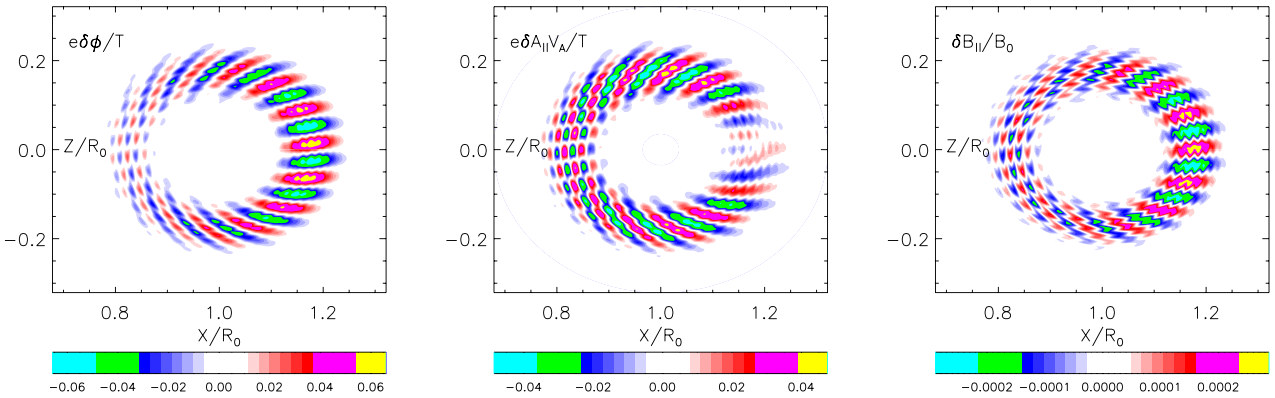

FIG. 6. KBM $\delta\phi$ (left), $\delta A_\parallel$ (middle), and $\delta B_\parallel$ (right) poloidal mode structure for $\beta_e = 0.02$, $k_\perp \rho_s = 0.22$.

$$\left(\rho_s^2\nabla_\perp^2 - \rho_s^4\nabla_\perp^4\right)\frac{e\delta\phi}{T} + \left(2\rho_s^2\nabla_\perp^2 - \rho_s^4\nabla_\perp^4\right)\frac{\delta B_\parallel}{B_0}$$
$$= -\left(1 - 2\rho_s^2\nabla_\perp^2 + \rho_s^4\nabla_\perp^4\right)\left(\frac{\delta n_i - \delta n_e}{n_0}\right),$$
$$\frac{\beta}{2}\left(2\rho_s^2\nabla_\perp^2 - \rho_s^4\nabla_\perp^4\right)\frac{e\delta\phi}{T} + [1 + 2\beta - (1+\beta)$$
$$\times\left(-2\rho_s^2\nabla_\perp^2 + \rho_s^4\nabla_\perp^4\right)]\frac{\delta B_\parallel}{B_0}$$
$$= -\frac{\beta}{2}\left(1 - 2\rho_s^2\nabla_\perp^2 + \rho_s^4\nabla_\perp^4\right)\left(\frac{\delta\tilde{P}_{i\perp} + \delta P_{e\perp}}{P_0}\right),$$

where $\delta\tilde{P}_i = 2\pi\Omega_i^2 \int d\mu dv_\parallel B_0 \langle \int_0^{\rho_i} F_i^{gyro} r dr \rangle$, $\beta = \beta_i = \beta_e$.

In the following simulations of tokamak plasmas, the terms on the order of β are neglected in the coupled equations, which become:

$$\frac{e\delta\phi}{T} = \left(1 - \rho_s^{-2}\nabla_\perp^{-2}\right)\frac{\delta n_i - \delta n_e}{n_0},$$
$$\frac{\delta B_\parallel}{B_0} = \frac{\beta}{2}\left[-\frac{\delta P_e + \delta\tilde{P}_i}{P_0} + \frac{\delta n_i - \delta n_e}{n_0} + \left(1 - \rho_s^2\nabla_\perp^2\right)^{-1}\frac{\delta n_i - \delta n_e}{n_0}\right].$$

A. Simulation parameters

To study the $\delta B_\parallel$ effects on low frequency instabilities driven by pressure gradients, linear KBM is simulated using GTC[30] with the cyclone parameters for the background plasmas: the major radius is $R_0 = 167$ cm and the inverse aspect ratio is $a/R_0 = 0.357$. At $r = 0.5a$, $B_0 = 2.01T$, $T_e = 8892eV$, $R_0/L_T = 6.9$, $R_0/L_n = 2.2$, $q = 1.4$. Simulations in this study use the lowest order $s - \alpha$ model with a circular cross-section as described in Ref. 11.

B. Simulation results

In the simulations, the toroidal mode number n is filtered and only a single n mode is kept in each simulation. The real frequency and the growth rate are calculated for the most unstable poloidal mode at the $q = 1.4$ flux surface. A mode number scan with $\beta_e = 0.02$ is shown in Fig. 5. Without $\delta B_\parallel$, the KBM growth rate decreases 23% at $k_\perp \rho_s = 0.22$, and the real frequency increases slightly. Thus, $\delta B_\parallel$ has a destabilizing effect on KBM. At $k_\perp \rho_s = 0.25$, with $\delta B_\parallel$ the mode linear growth rate agrees well with GS2 and GYRO results using the same parameters.[6] The results without $\delta B_\parallel$ is closer to the GYRO result in Ref. 6. The GS2 results in Ref. 2 show that the KBM growth rate decreases by a factor of 3 to 4 when neglecting only $\delta B_\parallel$ (but not the drift reversal term). The $\delta B_\parallel$ does not change the linear mode structures of the electrostatic and parallel vector potentials in these studies. The $\delta B_\parallel$ poloidal structure has similar features as the perturbed electrostatic potential $\delta\phi$ as shown in Fig. 6.

A β_e scan is shown in Fig. 7. As β_e becomes smaller, the KBM approaches the stability threshold, and the effects of $\delta B_\parallel$ on the mode real frequency become more significant. The mode evolves to the collisionless trapped electron mode (CTEM), followed by the ion temperature gradient (ITG) mode at $\beta_e < 1\%$. The simulations include the equilibrium current, which gives a positive drive to the KBM. At $\beta_e = 0.02$ and the poloidal mode number $k_\perp \rho_s = 0.22$, the KBM

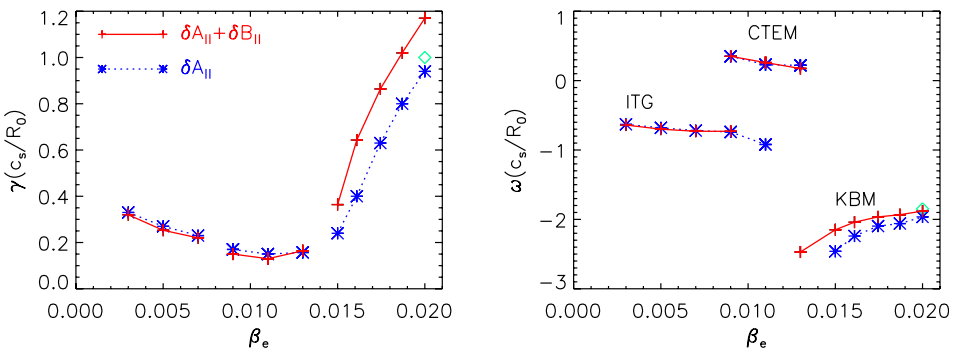

FIG. 7. KBM growth rate γ (left) and real frequency ω (right) vs β_e for poloidal mode number $k_\perp \rho_s = 0.22$. Green diamond data points represent simulation results with $\delta B_\parallel$ and without equilibrium current.

growth rate decreases 17% if equilibrium current terms are dropped, as shown by the green diamond data point in Fig. 7. At $\beta_e = 1.5\%$, the KBM growth rate with $\delta B_\parallel$ agrees with the GYRO result from Fig. 3 in Ref. 6. As β_e further decreases to 1.3%, both the KBM frequency and a positive frequency corresponding to CTEM are observed in the simulation with $\delta B_\parallel$. Whereas in the simulation without $\delta B_\parallel$, CTEM is the only unstable mode. At $\beta_e = 1.1\%$, the positive frequency corresponding to CTEM is observed in the case with $\delta B_\parallel$, and both frequencies corresponding to CTEM and ITG are observed in the case without $\delta B_\parallel$, showing that $\delta B_\parallel$ has a stabilizing effect on ITG near the stability threshold. As β_e becomes smaller than 1%, ITG becomes unstable with a negative frequency. At $\beta_e = 0.5\%$, the ITG growth rate agrees with the GYRO result from Fig. 2 in Ref. 6. The effect of $\delta B_\parallel$ becomes almost negligible for $\beta_e < 0.7\%$.

V. CONCLUSIONS AND FUTURE WORK

In this work, we have developed a simulation scheme for fluid kinetic hybrid electrons and gyrokinetic ions in toroidal geometry with parallel magnetic perturbation $\delta B_\parallel$, which was generally neglected in particle-in-cell simulations of fusion plasmas. A scan in β_e from 0.06 to 1.76 in the kinetic Alfven wave (KAW) simulations verifies the implementation of $\delta B_\parallel$ for a uniform isotropic background in slab geometry. Simulations of drift-Alfvenic instabilities in tokamak geometry show that $\delta B_\parallel$ has a destabilizing effect on the kinetic ballooning mode (KBM), consistent with theoretical predictions and other numerical studies.[2,6] $\delta B_\parallel$ does not have a significant effect on the linear properties of the collisionless trapped electron mode (CTEM), and has a stabilizing effect on ion temperature gradient (ITG) instability. Equilibrium current is included in the simulations, and it provides a positive linear drive for the KBM.

In future work, we will extend the formulation to anisotropic equilibrium, where the parallel Ampere's law might be modified by finite β effects.[9] $\delta B_\parallel$ can play an important role in the nonlinear dynamics of KBM,[31] therefore, incorporating $\delta B_\parallel$ in nonlinear simulations is an important next step.

ACKNOWLEDGMENTS

The authors acknowledge useful discussions with the GTC team. Research was supported by the U.S. DOE SciDAC GSEP and DOE Contract Nos. DE-AC02-09CH11466, DE-SC0014032, and DE-FG02-07ER46372. This research used resources of the Oak Ridge Leadership Computing Facility at Oak Ridge National Laboratory (DOE Contract No. DE-AC05-00OR22725) and the National Energy Research Scientific Computing Center (DOE Contract No. DE-AC02-05CH11231).

[1]E. Frieman and L. Chen, Phys. Fluids **25**, 502 (1982).
[2]N. Joiner, A. Hirose, and W. Dorland, Phys. Plasmas **17**, 072104 (2010).
[3]J. M. Canik, W. Guttenfelder, R. Maingi, T. H. Osborne, S. Kubota, Y. Ren, R. E. Bell, H. W. Kugel, B. P. LeBlanc, and V. A. Souhkanovskii, Nucl. Fusion **53**, 113016 (2013).
[4]W. M. Tang, J. W. Connor, and R. J. Hastie, Nucl. Fusion **20**, 1439 (1980).
[5]H. L. Berk and R. R. Dominguez, J. Plasma Phys. **18**, 31 (1977).
[6]E. A. Belli and J. Candy, Phys. Plasmas **17**, 112314 (2010).
[7]A. Brizard and T. S. Hahm, Rev. Mod. Phys. **79**, 421 (2007).
[8]A. Brizard, Phys. Fluids B **4**, 1213 (1992).
[9]P. Porazik and Z. Lin, Phys. Plasmas **18**, 072107 (2011).
[10]Z. Lin, T. S. Hahm, W. W. Lee, W. M. Tang, and R. B. White, Science **281**, 1835 (1998).
[11]W. Deng, Z. Lin, and I. Holod, Nucl. Fusion **52**, 023005 (2012).
[12]P. Porazik and Z. Lin, Commun. Comput. Phys. **10**, 899 (2011).
[13]W. W. Lee, Phys. Fluids **26**, 556 (1983).
[14]A. M. Dimits and W. W. Lee, J. Comput. Phys. **107**, 309 (1993).
[15]S. E. Parker and W. W. Lee, Phys. Fluids B **5**, 77 (1993).
[16]I. Holod, W. L. Zhang, Y. Xiao, and Z. Lin, Phys. Plasmas **16**, 122307 (2009).
[17]E. Startsev and W. W. Lee, Phys. Plasmas **21**, 022505 (2014).
[18]Y. Chen and S. E. Parker, J. Comput. Phys. **189**, 463 (2003).
[19]Z. Lin and L. Chen, Phys. Plasmas **8**(5), 1447 (2001).
[20]J. McClenaghan, Z. Lin, I. Holod, W. Deng, and Z. Wang, Phys. Plasmas **21**, 122519 (2014).
[21]D. Liu, W. Zhang, J. McClenaghan, J. Wang, and Z. Lin, Phys. Plasmas **21**, 122520 (2014).
[22]D. Liu, J. Bao, T. Han, J. Wang, and Z. Lin, Phys. Plasmas **23**, 022502 (2016).
[23]Y. Xiao and Z. Lin, Phys. Rev. Lett. **103**, 085004 (2009).
[24]L. Schmitz, D. P. Fulton, E. Ruskov, C. Lau, B. H. Deng, T. Tajima, M. W. Binderbauer, I. Holod, Z. Lin, H. Gota *et al.*, Nat. Commun. **7**, 13860 (2016).
[25]W. Zhang, Z. Lin, and L. Chen, Phys. Rev. Lett. **101**, 095001 (2008).
[26]H. S. Zhang, Z. Lin, and I. Holod, Phys. Rev. Lett. **109**, 025001 (2012).
[27]Z. Wang, Z. Lin, I. Holod, W. W. Heidbrink, B. Tobias, M. V. Zeeland, and M. E. Austin, Phys. Rev. Lett. **111**, 145003 (2013).
[28]G. Howes, S. C. Cowley, W. Dorland, G. W. Hammett, E. Quataert, and A. A. Schekochihin, Astrophys. J. **651**, 590–614 (2006).
[29]S. Balay, S. Abhyankar, M. F. Adams, J. Brown, P. Brune, K. Buschelman, V. Eijkhout, W. D. Gropp, D. Kaushik, M. G. Knepley, L. C. McInnes, K. Rupp, B. F. Smith, and H. Zhang, PETSc Web page, 2014.
[30]I. Holod and Z. Lin, Phys. Plasmas **20**, 032309 (2013).
[31]W. Guttenfelder, J. L. Peterson, J. Candy, S. M. Kaye, Y. Ren, R. E. Bell, G. W. Hammett, B. P. LeBlanc, D. R. Mikkelsen, W. M. Nevins, and H. Yuh, Nucl. Fusion **53**, 093022 (2013).